Morphological Study and Melting Behavior of Narrow Molecular Weight Fractions of Poly(aryl ether ether ketone) (PEEK) Annealed from the Glassy State

C. Fougnies,[†] M. Dosière,*[,†] M. H. J. Koch,[‡] and J. Roovers[§]

Laboratoire de Physicochimie des Polymères, Université de Mons-Hainaut, Place du Parc, 20, B-7000-Mons, Belgium, Hamburg Outstation, European Molecular Biology Laboratory, EMBL c/o DESY, Notkestrasse 85, D-22603 Hamburg, Germany, and Institut de Technologie et de Recherche Environnementale, National Research Council, Ottawa, K1A OR6, Canada

Received April 22, 1998; Revised Manuscript Received June 22, 1998

ABSTRACT: The morphology of several semicrystalline poly(aryl ether ether ketone) (PEEK) samples with narrow molecular weight distributions and of a commercial sample of PEEK has been investigated by means of differential scanning calorimetry (DSC), wide-angle X-ray diffraction (WAXD), and small-angle X-ray scattering (SAXS). The use of different molecular weights allows us to enlarge the macroscopic crystallinity range usually attainable for the commercial PEEK grades. WAXD and DSC data are in good agreement to estimate the weight degree of crystallinity values ranging from ∼15% for the highest molecular weight sample to ∼55% for the lowest molecular weight sample. Most of the investigated samples exhibit the well-known double melting behavior with a low and a high melting endotherm. This behavior is interpreted in the light of a melting−recrystallization mechanism which is strongly affected by the presence of entanglements in the amorphous zones. The analysis of the SAXS data shows that, under constant annealing conditions, the crystal thickness (given by the smallest length obtained from the correlation function) remains unaffected by a change of the molecular weight while the amorphous layer is found to strongly increase with increasing chain length due to the presence of entanglements. This leads to a decrease in the linear degree of crystallinity within the lamellar stacks which is consistent with the behavior of the macroscopic degree of crystallinity obtained from WAXD, DSC, and density measurements.

Introduction

Poly(aryl ether ether ketone) (PEEK) is a high-temperature aromatic polymer with very good thermal and mechanical properties combined with excellent chemical resistance.[1−3] It can be obtained either in a fully amorphous state by quenching from the melt or in a semicrystalline state by annealing from the glassy state or crystallization from the melt. Since its synthesis, a large number of publications was devoted to its crystallization and melting behaviors as well as to the morphology of semicrystalline samples. Most of these studies were made by differential scanning calorimetry (DSC),[4−13] small-angle X-ray scattering (SAXS), and wide-angle X-ray diffraction (WAXD) including time-resolved experiments,[13−27] thermomechanical analysis,[29−32] transmission electron microscopy (TEM),[11,33−36] and optical microscopy (OM).[37,40]

The melting curve of a semicrystalline sample of PEEK generally contains two endotherms which have led to two major and antagonistic hypotheses concerning their origin: (i) the complex melting arises from the presence of two distinct lamellar populations present in the sample before the DSC scan and melting at different temperatures;[6,11,23,24] (ii) the sample contains only one population of crystals starting to melt at the temperature of the first endotherm and then continuously reorganizing during the scan, with the high-temperature endotherm representing the final melting of the recrystallized lamellae.[4,7,28] A compromise between these two extremes has been also proposed.[9] The two hypotheses were suggested mainly from DSC measurements and a complementary analysis of the morphology. It was found that PEEK crystallizes in lamellar stacks amorphous zones alternating with lamellar crystals of limited lateral size. No unequivocal evidence was yet presented in favor of either of these hypotheses. If a two-phase model with amorphous and crystalline regions is used to describe the lamellar stacks, the correlation function of the SAXS intensity data yields two thicknesses L_1 and L_2[41,42] (with $L_1 > L_2$) the sum of which is equal to the long period L_p. The assignment of the crystal thickness (L_c) to L_1 or to L_2 has to be made on the basis of other information. This has unfortunately led to a controversy which did not help in the elucidation of the melting process as the crystal thickness L_c was in some cases attributed to the shortest (L_2)[21,26−28] and in others to the largest (L_1)[23,24] length obtained from the analysis of the SAXS correlation function. Despite several studies devoted to this topic, the question was not settled. It is generally accepted that almost all the properties of the bulk crystallized polymers are affected by their molecular weight distribution. In particular, the lamellar morphology has been shown to strongly depend on the molecular chain length for flexible as well as for stiff polymers.[43,44] For PEEK, most of the published literature concerns industrial grade materials, generally with broad molecular weight distributions. Only a few studies were devoted to the influence on the molecular weight of PEEK on its properties. The mechanical properties were found to be strongly dependent on the average molecular weight for polydisperse industrial PEEK samples.[32] The melt-

[†] Université de Mons-Hainaut.
[‡] European Molecular Biology Laboratory.
[§] National Research Council.

S0024-9297(98)00640-8 CCC: $15.00
Published on Web 08/19/1998

Table 1. Main Characteristics of the Different PEEK Samples: Number Average Molecular Weight ($\bar{M}_n$), Weight Average Molecular Weight ($\bar{M}_w$), Number Average Chain Length ($\bar{l}_n^{ext}$) and Weight Average Chain Length ($\bar{l}_w^{ext}$), Glass Transition Temperature (T_g), Cold Crystallization Temperature (T_{cc}), Temperature Where the Overall Crystallization Rate Is Equal to the Overall Melting Rate (T^*) and Estimated Equilibrium Melting Temperature (T_m^0)

sample	$\bar{M}_n$	$\bar{M}_w$	$\bar{l}_n^{ext}$ (nm)	$\bar{l}_w^{ext}$ (nm)	T_g (°C)	T_{cc} (°C)	T^* (°C)	T_m (°C)	T_m^0 (°C)[c]
4k	3500[b]	4400[b]	18	23	122.5	152.5	315	344.0	417
8k	7000[b]	8300[b]	36	43	133.5	165.5	324	350.5	400
18k	14500[b]	18000[b]	75	94	140.0	176.0	307	349.0	402
32k	21500[b]	32000[b]	111	166	145.5	183.5	288	339.0	447
79k	60200[b]	79500[b]	313	414	147.5	190.5	273	325.0	424
Stabar K200	35000−50000[a]	95000−120000[a]	180−260	500−620	143.0	175.0	300	339.8	496

[a] From ref 51. [b] From ref 50. [c] From the Hoffman−Weeks plot.[60]

ing behavior of an industrial grade PEEK and a laboratory-made low molecular weight PEEK were found to be different.[45] Very short oligomers of PEEK were also investigated in a attempt to understand the physical properties of the corresponding polymer, and their complex melting behavior was related to difference in the position of ether and ketone bridges in the crystal.[46] For poly(aryl ether ketone) or PEK, a similar thermoplastic, the morphology of single crystals and in particular the chain folding were found to drastically depend on the molecular weight.[47] The large loss in crystal perfection when going from the extended chain to the folded oligomers was attributed to the stiffer character of the polymer chains. Finally the kinetics of crystallization of several narrow molecular weight fractions of PEEK covering a large range of molecular weights was studied by means of differential scanning calorimetry and optical microscopy.[48,49] The spherulitic growth as well as the bulk crystallization rate depends on the molecular weight.

A study of the morphology of semicrystalline samples of PEEK in relation to their molecular weight would greatly help to understand their semicrystalline properties as well as their melting behavior. The present work concerns a DSC, WAXD, and SAXS study of several narrow PEEK fractions cold crystallized from the glassy state and further annealed at temperature between 250 and 340 °C.

Experimental Section

Materials. Several monodisperse samples of PEEK were synthesized and characterized as described elsewhere.[50] The molecular characteristics of Stabar K200 were taken from the work of Bas *et al.*[51] Throughout the present paper, the weight average molecular weight $\bar{M}_w$ is used to characterize the materials and is referred to as 18k for a weight average molecular weight of 18 000. Amorphous films of these fractions were obtained by melting the powders into a laboratory press (Carver) heated at 400 °C for 1 min followed by rapid quenching in an ice−water mixture. The so-obtained films were found to be amorphous as checked by wide-angle X-ray diffraction. The commercial grade of PEEK Stabar K200 used in this study was supplied by ICI in the form of amorphous 0.250 mm thick films. The main characteristics of the various samples are given in Table 1.

Annealing Experiments. Semicrystalline samples were prepared in a Mettler FP82HT hot stage by heating amorphous films at 10 °C/min from 100 °C to the annealing temperature T_a. The samples were annealed for 1 h at temperatures between 250 and 340 °C and subsequently cooled to room temperature at −10 °C/min.

Differential Scanning Calorimetry (DSC). The DSC measurements were made at a scanning rate of 10 °C/min in a heat flux differential scanning calorimeter (TA Instruments, Model 2920) working under nitrogen atmosphere using about 2 mg of each sample. Temperature and heat flow calibrations were done using caffeine, indium, and zinc. A new baseline was recorded by running two empty pans before each set of three melting experiments. The melting heat of PEEK was taken as the area over a linear baseline drawn from just above the glass transition to a temperature above the second melting endotherm.[52] The weight degree of crystallinity was computed using a value of 130 J/g for the crystalline melting enthalpy of PEEK.[4]

Density Measurements. The density of some of PEEK films was determined by the flotation technique in aqueous calcium nitrate solutions. The density of the solutions was measured with a precision of 10^{-4} g/cm^3 at 25 °C using a Mettler DA300M specific gravity meter. No density measurements were possible for the other molecular weight fractions due to the difficulty in obtaining sufficiently large samples free of air bubbles.

X-ray Diffraction. Ni-filtered Cu Kα radiation from a point focus rotating anode (Rigaku RU200) was used to record the WAXD patterns on image plates with a modified Kiessig camera (pinhole collimation). The image plates were scanned with a FujiX BAS-3000 imaging analyzer. The image reader yields 12 bits intensity data with a resolution of (50 μm)^2. The area of the square image plate is around 140 cm^2. The range of scattering vector is 1/(1.5 nm) < s < 1/(0.45 nm) ($s = 2(\sin\theta)/\lambda$ where 2θ is the scattering angle and λ the wavelength of the incident X-ray beam (0.15418 nm)). The following operations were performed on these area detector data using the "X-ray" software:[53] (i) automatic search of the center of the X-ray pattern; (ii) background subtraction; (iii) Lorentz and polarization corrections; (iv) angular integration of the pattern to obtain intensity profiles; (v) analysis of the intensity profiles: peak fitting and integration; (vi) determination of the parameters of the unit cell.

The SAXS curves were recorded in 180 s with a linear position detector on the X33 beam line of the EMBL in HASYLAB on the storage ring DORIS III of the Deutsche Elektronen Synchrotron (DESY) at Hamburg, Germany.[54,55] The SAXS intensities were recorded in the range 1/(70 nm) < s < 1/(3 nm). The wavelength of the incident synchrotron X-ray beam was 0.15 nm. The calibration of the detector channels in terms of scattering vector was made by linear regression over the positions of the first twelve orders of collagen fibers (L_p = 65 nm). To evaluate the correlation function $\gamma(r)$, the fluidlike contribution was estimated from a plot of Is^4 versus s^4 and subtracted before extrapolating the SAXS intensity curves to large s-values using Porod's law.[56] The SAXS curves were Lorentz corrected by multiplying the intensity data by s^2. The lamellar thickness L_c, the amorphous thickness L_a, the long period L_p and the linear degree of crystallinity v_c^{lin} were obtained according to standard procedures.[41,42] It was not possible to accurately determine the amount of material effectively irradiated by the incident X-ray beam in the SAXS synchrotron measurements because the small quantities of material available for the different polymer fractions precluded the preparation of samples of uniform size and constant thickness.

Results and Discussion

Relationship between the Glass Transition and the Melting Temperature of PEEK Fractions and

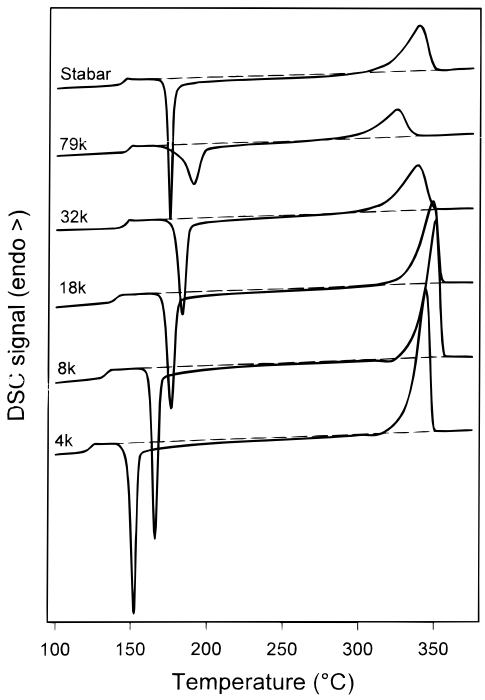

Figure 1. DSC heating curves of amorphous PEEK fractions and amorphous Stabar. The values of the average molecular weight of the fractions are inserted in the figure. The curves are shifted for clarity.

Their Molecular Weights. The DSC curves of the initially amorphous PEEK fractions investigated here are shown in Figure 1 and are very close to those already published by Day *et al.*[48] The evolution of the glass transition temperature T_g with the molecular weight was interpreted using Ueberreiter and Kanig's law,[57] and although the increase of the cold crystallization temperature T_{cc} was discussed, the large decrease of the melting temperature T_m with increasing molecular weight was unnoticed (Table 2). Such a behavior provides a clear evidence for a reorganization process involving continuous melting of lamellar crystals and subsequent recrystallizaton during heating of PEEK samples. The number of entanglements in the amorphous zones must be very small in the 4k and 8k PEEK fractions used here. Therefore, the chain mobility is certainly large and allows reorganization of the cold crystallized lamellae over a wide range of temperature. In contrast, for the high molecular weight samples the rate of recrystallization is considerably lowered by the presence of entanglements at the growth front, which strongly hinder the reorganization of the lamellae. Consequently, the melting process dominates at relatively low temperatures, with the short chains having the highest melting rate. This is also shown for the various PEEK fractions by the decrease of the temperature T^* at which the overall crystallization rate equals the overall melting rate with increasing molecular weight (Table 2). The exothermic contribution, i.e., the recrystallization, becomes a minor process at low temperatures for the longest chains.

The influence of the increase of the number of entanglements on the melting behavior of PEEK fractions parallels the effect of electron irradiation on the amorphous zones. The melting temperature of electron irradiated PEEK samples decreases with increasing radiation dose and thus the degree of cross-linking.[58] The temperatures of the glass transition and of the extremum of the cold crystallization peak are both shifted upward while the heats of crystallization and melting decrease (Figure 3 in ref 58).

Relationship between the Melting of PEEK Fractions Annealed from the Glassy State and Their Molecular Weight. The melting curves of semicrystalline PEEK fractions annealed at 280, 300, and 320 °C from the glassy state are shown in parts a−c of Figure 2, respectively. The DSC curves of the 8k and 79k samples annealed at seven different temperatures are shown in parts a and b of Figure 3, respectively. These samples as well as the other PEEK fractions investigated in this work exhibit the well-known double melting behavior with a low (endotherm I characterized by a peak temperature T_m^I) and a high (endotherm II characterized by a peak temperature T_m^{II}) melting endotherms. This behavior has already been described in detail for industrial grades of PEEK and can be attributed to a reorganization at least at the low annealing temperatures. For the high annealing temperatures, however, a two-step crystallization process takes place: an isothermal crystallization during the 1 h annealing and a nonisothermal crystallization during cooling to room temperature. The latter thermal treatment also leads to two endotherms resulting from the melting of two lamellar populations as illustrated, for example, for the high molecular weight PEEK fraction (79k) annealed at 330 °C in Figure 3b. For a commercial grade PEEK (Stabar), the minimum annealing temperature at which there is significant crystallization during cooling is 340 °C.[28] For the PEEK fractions investigated here, this temperature decreases and this restricts the range for which only annealing occurs at higher molecular weights. This is illustrated by the 79k fraction for which crystallization occurs during cooling after isothermal annealing at 330 °C. This behavior can be attributed to an incomplete crystallization during the isotherm due to the reduced rate of crystallization resulting from the higher viscosity. In contrast, with the polydisperse PEEK samples, a process of molecular weight segregation cannot easily be invoked as the origin of the nonisothermal crystallization of the sharp fractions.

The melting temperatures of both endotherms are plotted in Figure 4 as a function of the annealing temperature for experiments where crystallization during the cooling is negligible or absent (see also Table 2). The temperature of the high temperature melting peak strongly depends on the molecular weight (parts a−c of Figure 2) but seems to be almost independent of the annealing temperature (parts a and b of Figure 3). This is true as long as the annealing is performed in a temperature range where no significant melting takes place during the heating from 100 °C to the annealing temperature (i.e. below the endotherm present in the DSC curve of the initially amorphous sample in Figure 1). The shape of endotherm II is identical (even if partly masked by endotherm I) to that of the melting peak of the initially amorphous sample which nonisothermally cold crystallizes during the DSC scan (Figure 1) for all fractions annealed in this temperature range (T_a = 250−300 °C for the 79k sample for example). The high-temperature endotherm thus corresponds to the melting of an identical population of lamellae in samples with a given average molecular weight. This supports the hypothesis of a reorganization mechanism proposed earlier.[27,28]

Table 2. First Melting Peak Temperature (T_m^I), Second Melting Peak Temperature (T_m^{II}), Total Melting Heat (ΔH^m), Mass Degree of Crystallinity Estimated by DSC (W_c^{DSC}), by Density Measurements (W_c^{dens}), and by WAXD (W_c^{WAXD}), Bragg Long Period (L_p^{Bragg}), Long Period Computed from the Correlation Function ($L_p^{\gamma(r)}$), Crystalline Layer Thickness ($L_c = L_2$), and Linear Crystalline Fraction (v_c^{lin}) for the PEEK Samples Annealed at Different Annealing Temperature (T_a)

sample	T_a (°C)	T_m^I (°C)	T_m^{II} (°C)	ΔH_m (J/g)	W_c^{DSC} (%)	W_c^{dens} (%)	W_c^{WAXD} (%)	L_p^{Bragg} (nm)	$L_p^{\gamma(r)}$ (nm)	$v_2^{lin} = v_c^{lin}$	$L_2 = L_c$ (nm)
4k	250	264.0	346.3	69.5	53.5		47.4	7.9	7.5	0.41	3.1
	280	291.9	345.8	77.9	59.9		50.5	8.4	8.0	0.41	3.3
	300	310.4	345.8	79.3	61.0		52.0	8.9	8.5	0.40	3.4
	310	320.2	345.6	75.7	58.3		54.2	9.6	9.1	0.40	3.6
	320	329.8	344.7	77.5	59.6		55.5	10.7	10.1	0.36	3.6
	330	339.0	343.9	76.5	58.8		56.3	12.2	11.4	0.36	4.1
	340	347.2[a]		84.8	65.3		55.9	14.2	13.2	0.35	4.6
8k	250	264.7	350.2	61.5	47.3		39.4	9.0	8.3	0.35	2.9
	280	292.4	350.3	62.4	48.0		43.0	9.5	8.8	0.35	3.1
	300	311.2	350.0	67.9	52.2		45.0	9.8	9.3	0.36	3.3
	310	320.7	349.7	74.1	57.0		46.7	10.3	9.7	0.35	3.4
	320	328.5	349.5	76.5	58.8		48.5	10.9	10.2	0.35	3.6
	330	338.4	348.9	72.6	55.9		50.8	12.1	11.3	0.35	3.9
	340	346.7	347.0[c]	69.1	53.2		50.1	13.4	12.5	0.32	4.0
18k	250	264.5	348.5	51.2	39.4		33.4	10.3	9.5	0.33	3.1
	280	292.1	348.7	47.0	36.2		37.0	10.8	10.2	0.37	3.8
	300	312.2	348.5	56.2	43.2		39.5	11.2	10.6	0.31	3.3
	310	321.0	347.6	61.0	46.9		40.7	11.5	10.9	0.31	3.4
	320	330.0	347.6	57.0	43.8		42.4	12.1	11.4	0.32	3.7
	330	338.5	346.0	61.8	47.5		43.3	13.1	12.3	0.33	4.0
	340	347.5[a]		58.2	44.8		44.6	14.6	13.7	0.31	4.3
32k	250	267.8	339.4	45.7	35.2		29.6	11.2	10.6	0.29	3.1
	280	296.2	338.4	51.3	39.4	32.8	32.9	11.8	11.4	0.27	3.1
	300	318.8	335.6	47.3	36.4		36.5	12.6	12.0	0.29	3.5
	310	326.3	333.0[c]	62.0	47.7	35.5	35.8	13.0	12.6	0.28	3.5
	320	335.3		57.3	44.1		34.7	13.9	13.2	0.28	3.7
	330	345.0[a]		40.1	30.9		32.0	15.8	15.3	0.28	4.3
	340	356.5[a]		24.3	18.7	20.0	25.2	18.2	16.3	0.23	3.8
79k	250	264.7	326.0	33.3	25.6	25.5	24.8	12.8	12.0	0.27	3.2
	280	295.5	325.9	33.2	25.5	26.0	26.0	14.3	14.0	0.24	3.4
	300	318.3	325.4	37.6	28.9	25.0	27.9	14.7	15.0	0.22	3.3
	310	326.0[a]		32.3	24.8	22.5	28.0	15.6	15.0	0.25	3.8
	320	334.8[a]		24.4	18.8	24.5	26.9	16.1	15.9	0.25	3.9
	330	343.9[a]		22.3	17.2	20.0	24.5	15.6	15.8	0.25	4.0
	340	311.0[b]		16.1	12.4	15.5	20.1	16.3	16.0	0.24	3.9
Stabar	250	264.0	340.5	42.3	32.5		30.5	11.3	10.9	0.28	3.1
	280	291.9	340.0	41.3	31.8	30.0	31.4	12.1	11.6	0.28	3.2
	300	310.4	340.3	42.1	32.4	31.5	34.3	12.6	12.0	0.28	3.3
	310	320.2	340.1	45.6	35.1	33.0	35.2	13.0	12.4	0.27	3.4
	320	329.8	339.0	49.5	38.1	34.5	35.5	13.5	12.9	0.29	3.7
	330	339.0[a]		55.9	43.0	36.5	38.9	14.4	13.6	0.29	4.0
	340	348.3[a]		60.4	46.5	39.0	40.0	15.1	14.3	0.30	4.3

[a] Only one high temperature melting endotherm and one broad melting endotherm corresponding to nonisothermally crystallized material. [b] Only one broad melting endotherm corresponding to nonisothermally crystallized material. [c] Shoulder.

In contrast, the position of the low-temperature endotherm seems to be almost independent of the chain length for a given annealing temperature (Table 2 and Figure 4). This suggests that in these samples, the lamellar crystals formed at constant annealing temperature T_a start to melt and reorganize approximately at the same temperature independent of the molecular weight, giving rise to the low-temperature endotherm peaking around 15 °C above the crystallization temperature T_a. The small increase of T_m^I between the small (4k, 8k, 18k) and the high molecular weight fractions (32k and 79k) can be explained as follows: as recrystallization is more difficult for the high molecular weight samples (32k and 79k), the exothermic contribution occurs in a narrower temperature range leading to a small shift of the first melting peak to higher temperature. Finally at the end of the DSC scan, as in the case of the initially amorphous samples, the reorganization process stops at lower temperature for the high molecular weight fractions because the number of entanglements is larger, which shifts endotherm II to lower temperatures.

For the high annealing temperatures (T_a = 310−340 °C for the 79k, for example), reorganization of the lamellae is no longer possible at the heating rate (10 °C/min) used in the experiments. The remaining sharp peak is thus characteristic of the melting of isothermally crystallized lamellar crystals. The broad low temperature melting peak is due to the melting of nonisothermally crystallized lamellar crystals as already mentioned.

Our results are in complete agreement with a recent study on the crystallization of poly(phenylene sulfide) (PPS) from the glassy state which demonstrated by modulated differential scanning calorimetry (MDSC) and dynamic mechanical analysis (DMA) that the molecular weight is a determining factor affecting the reorganization mechanism and/or the crystallization mechanism.[59] More precisely, the analysis of the nonreversing heat flow curves shows that low molecular weight PPS reorganizes over a wide range of temperatures while the high molecular weight samples have a much lower recrystallization rate, which restricts the reorganization to lower temperatures.

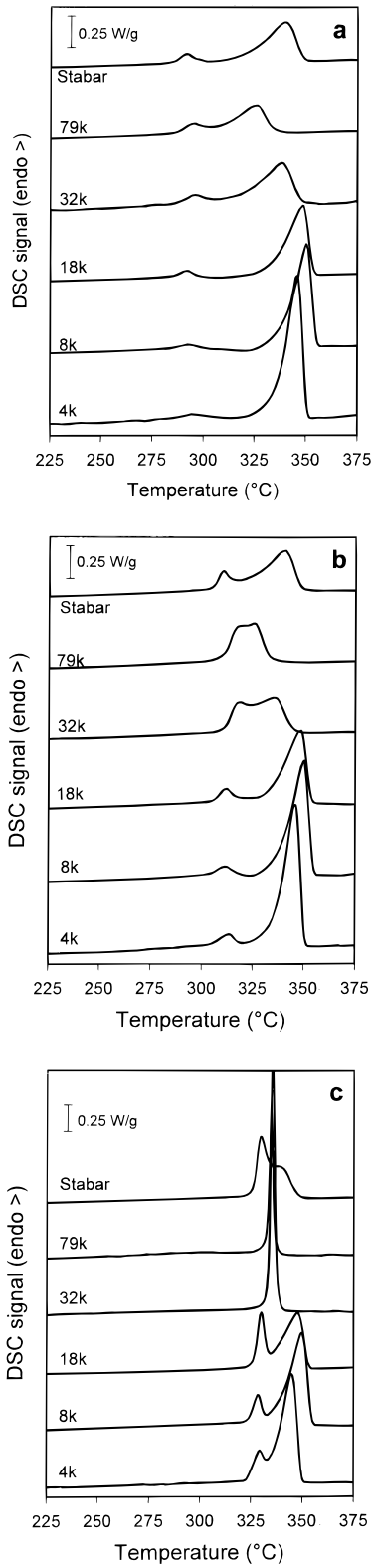

Figure 2. DSC heating curves of PEEK fractions and Stabar crystallized from the glassy state during 1 h at 280 °C (a), 300 °C (b), and 320 °C (c). The values of the weight average molecular weight of the fractions are inserted in the figures. The curves are shifted of clarity.

Equilibrium Melting Temperature of PEEK. In an attempt to determine the equilibrium melting temperature T_m^0 of PEEK, the melting temperature T_m^I was plotted against the annealing temperature T_a (Figure 4). According to the Hoffman−Weeks theory,[60] the intersection of the linear regressions of T_m^I versus T_a and $T_m = T_a$ should yield T_m^0. The extrapolated values are listed in Table 1 for the different PEEK fractions. For the low molecular weight fractions, this method yields values ranging from 400 to 417 °C which are in rather good agreement with the value usually quoted.[4,9,12] In contrast, the extrapolated values appear to be meaningless for the two high molecular weight samples as well as for the Stabar industrial grade sample. The Hoffmann−Weeks method thus seems inadequate to obtain accurate values of the equilibrium melting temperature T_m^0 for PEEK probably to due reorganization which precludes the determination of the true melting points even for the shorter chains.[9]

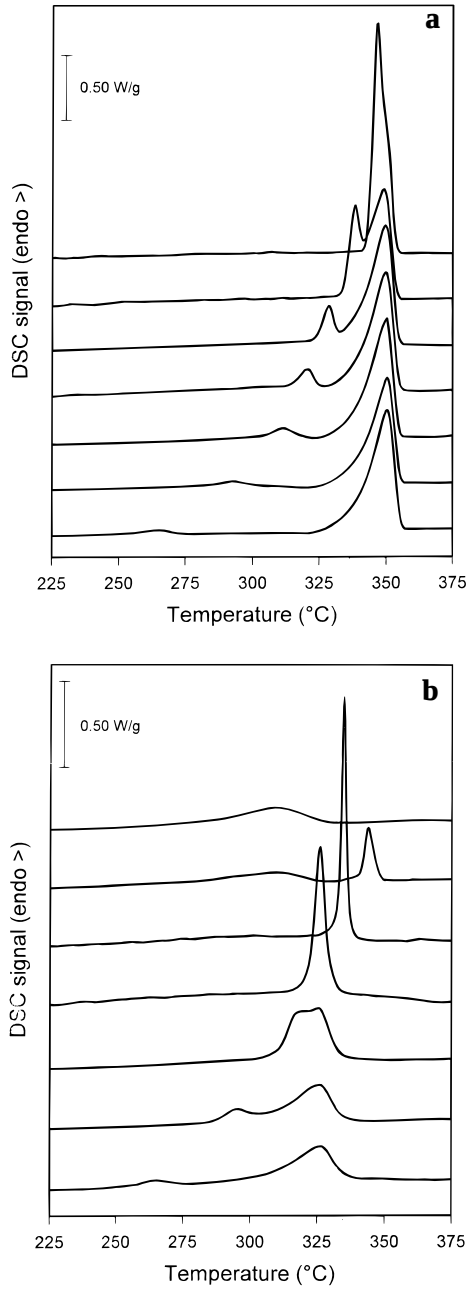

Figure 3. DSC curves of the PEEK 8k (a) and 79k (b) fractions crystallized from the glassy state during 1 h at 250, 280, 300, 310, 320, 330, and 340 °C (from bottom to top; the curves are shifted for clarity).

Degree of Crystallinity of Semicrystalline PEEK Fractions. On the basis of the commonly accepted value of 130 J/g for the heat of fusion of 100% crystalline PEEK,[4] the weight degree of crystallinity W_c^{DSC} can be

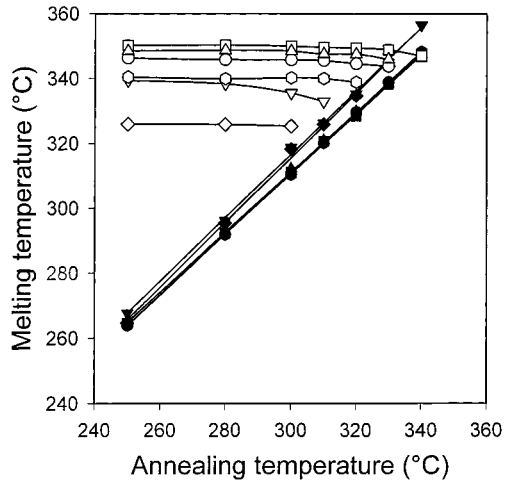

Figure 4. Peak temperature of the first melting endotherm (filled symbols) and of the second melting endotherm (open symbols) against the annealing temperature for the various PEEK fractions (●, ○) 4k, (■, □) 8k, (▲, △) 18k, (▼, ▽) 32k, (◆, ◇) 79k, and (⬢, ⬡) Stabar.

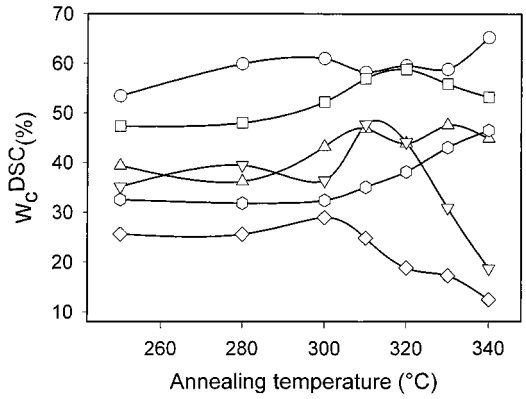

Figure 5. Weight degree of crystallinity of PEEK samples calculated from DSC data versus the annealing temperature: (○) 4k, (□) 8k, (△) 18k, (▽) 32k, (◇) 79k, and (⬡) Stabar.

estimated from the heat of fusion ΔH_m (the sum of the two endoterms) of the semicrystalline samples (Table 2). W_c^{DSC} increases over the whole range of annealing temperatures for the three low molecular weight samples (Figure 5) while it reaches a maximum value for the two high molecular weight samples for annealing temperatures around 300−310 °C. Although the average molecular weight of the Stabar polydisperse PEEK lies between that of the 32k and the 79k samples, its degree of crystallinity continuously increases between $T_a = 150$ and 340 °C. This probably reflects the presence of nonnegligible amounts of low molecular weight macromolecules which can reorganize even at high temperature during the thermal preparation of the sample. The PEEK fractions have degrees of crystallinity ranging from 0.15 to 0.60 corresponding to our knowledge to the widest range ever investigated for PEEK.

The degree of crystallinity of the PEEK fractions annealed between 250 and 340 °C have been determined from the WAXD intensity curves (Figure 6a). The weight degree of crystallinity W_c^{WAXD} was computed from the WAXD diffraction profile by subtracting a scaled diffraction profile obtained from an amorphous sample. The W_c^{WAXD} values in Table 2 are in close agreement with those obtained by thermal analysis and by density measurements. The evolution of W_c^{DSC} (Figure 5) and W_c^{WAXD} (Figure 7) with the annealing

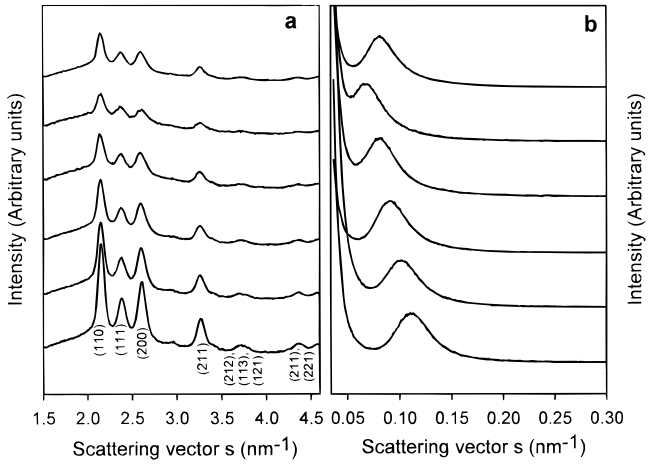

Figure 6. WAXD (a) and SAXS (b) intensity curves of various PEEK samples annealed from the glassy state at 300 °C during 1 h (from bottom to top: 4k, 8k, 18k, 32k, 79k, and Stabar; the curves are shifted for clarity). The Miller indices of the peaks are inserted in the figure.

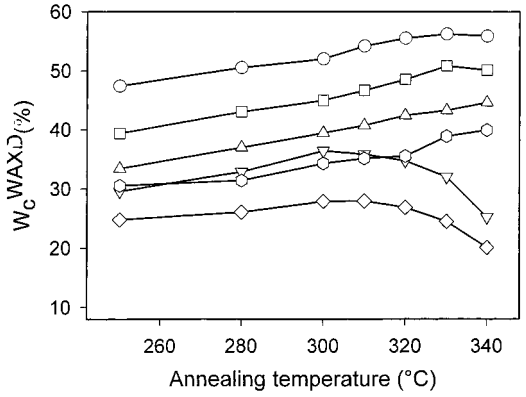

Figure 7. Weight degree of crystallinity of PEEK samples calculated from WAXD data versus the annealing temperature (○) 4k, (□) 8k, (△) 18k, (▽) 32k, (◇) 79k, and (⬡) Stabar.

temperature T_a for the various PEEK fractions are in agreement—the same trends leading to the same conclusions.

Crystal Density of PEEK Fractions. The Bragg spacings obtained from the diffraction profiles of all molecular weight fractions are characteristic of the orthorhombic unit cell of PEEK without any evidence for a different allotropic species. The unit cell parameters are plotted against the annealing temperature in Figure 8. As already reported for PEEK samples annealed from the glassy state or crystallized from melt, the unit cell density increases with annealing temperature.[62,63] However, for all annealing temperatures, the values of the crystallographic parameters *a*, *b*, and *c* are smaller for the 4k and 8k PEEK fractions than for the other samples. Moreover the *b*-axis, which is usually almost independent of the annealing conditions, decreases for these fractions. Consequently, the corresponding crystal densities are relatively high, reaching values of 1.405 g/cm^3 for the highest annealing temperatures. This may be due to a closer packing of the chains for these short oligomers with a better alignment of the ether and ketone bridges already invoked to explain the increase in density of the unit cell. The greater crystal perfection of the low molecular weight is also shown by the evolution of the peak width of the WAXD reflections. For a given annealing temperature, the reflections broaden with increasing molecular weight,

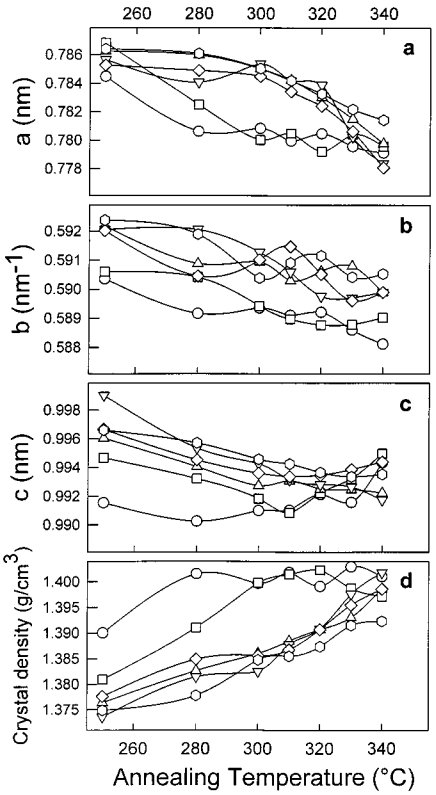

Figure 8. Crystallographic parameters *a* (a), *b* (b), and *c* (c) and crystal density (*d*) of the various PEEK samples against the annealing temperature (○) 4k, (□) 8k, (△) 18k, (▽) 32k, (◇) 79k, and (⬡) Stabar.

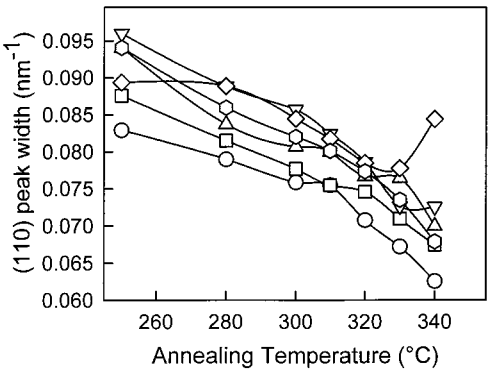

Figure 9. Width at half-height of the (110) diffraction as a function of the annealing temperature for the different PEEK samples (○) 4k, (□) 8k, (△) 18k, (▽) 32k, (◇) 79k, and (⬡) Stabar.

indicating a higher mosaicity of the crystals as shown in Figure 9 for a (110) diffraction. The constrained amorphous crystal interface may also play an important role by modifying the unit cells on the edge of the crystals.

Morphology of Lamellar Crystals of PEEK Fractions. SAXS curves corresponding to an annealing temperature of 300 °C are shown in Figure 6b for the different fractions. The maximum of the SAXS peak shifts to lower angles with increasing molecular weight which is associated with an increase of the long period L_p. A similar behavior is observed for the other annealing temperatures. Figure 10 illustrates that the Bragg long period L_p of all PEEK fractions increases with annealing temperature as expected. The behavior of the polydisperse Stabar sample is closest to that of the 32k fraction. An increase of the long period with

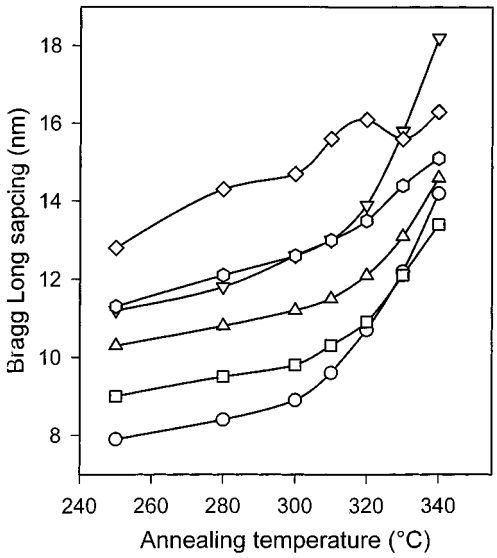

Figure 10. Bragg long spacing (calculated from the Lorentz corrected SAXS intensity curves) of the various PEEK samples against the annealing temperature (○) 4k, (□) 8k, (△) 18k, (▽) 32k, (◇) 79k, and (⬡) Stabar.

the molecular weight has already been reported for various polymers.[43,44] It is related either to an increase of the amorphous layer thickness (L_a), the crystalline layer thickness (L_c) or the two spacings L_c and L_a simultaneously. As often shown for polydisperse PEEK, the morphological parameters can be obtained from the linear correlation function $\gamma(r)$ calculated from the SAXS data. This procedure does not unambiguously yield the crystalline and amorphous thicknesses but only two lengths L_1 and L_2 (with $L_1 > L_2$) which must be assigned on the basis of independent information. We maintain our previous assignment[27,28] of the smallest value L_2 to the crystalline thickness L_c. This choice implies as discussed below that the linear degree of crystallinity $v_c^{lin} = L_c/(L_c + L_a)$ is generally smaller than 0.5. Our assignment is based on the following arguments. (i) For physical reasons, some authors claimed that thin lamellae including only a few chemical repeating units along the *c*-axis could not exist in semicrystalline PEEK. The correlation function analysis generally yielding values of L_1 and L_2 around 7.5 and 3.5 nm, respectively, they assigned the larger length i.e., L_1, to the crystalline layer thickness L_c. In the present case, the long periods L_p obtained for the two lowest molecular weight fractions range from ∼7.0 to ∼9.0 nm for annealing temperatures in the range 250−300 °C (Table 2). The analysis of the correlation functions gives $L_1 \cong 4-5$ nm and $L_2 \cong 3-4$ nm (Table 2 and Figure 11). As one of these two sets of data must correspond to the crystalline layer, this gives clear evidence that lamellar thicknesses as low as 4 nm (i.e., approximately three chemical repeating units) can occur in semicrystalline PEEK samples. For these low molecular weight fractions with relatively high degrees of crystallinity, the correlation functions were computed without difficulty as the scattering patterns have a high quality because the scattering maximum occurs at large Bragg angles. (ii) At constant annealing temperature, L_2 is found to be almost independent of the molecular weight of the PEEK fraction while the value of L_1 strongly increases with increasing molecular weight (Figure 10). For experiments carried out at a given annealing temperature and characterized by the same degree of supercooling, one would expect the crystalline thickness L_c

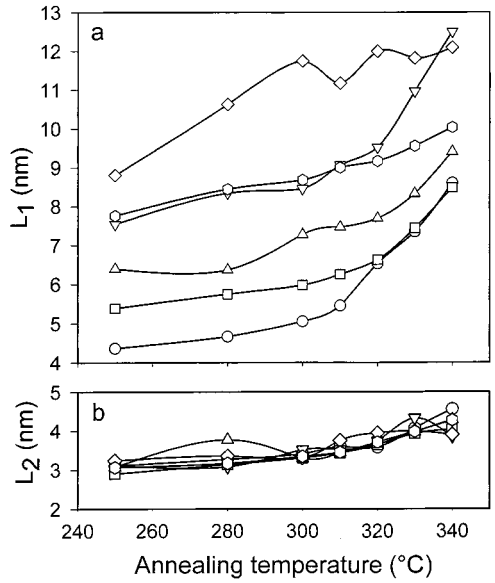

Figure 11. Thicknesses L_1 (a) and L_2 (b) obtained from the analysis of the SAXS correlation function of various PEEK samples against the annealing temperature (○) 4k, (□) 8k, (△) 18k, (▽) 32k, (◇) 79k, and (⬡) Stabar.

to be independent of the molecular weight. If there is an increase of the equilibrium melting temperature T_m^0 with the molecular weight as estimated by Day *et al.*,[48] one would expect a simultaneous small decrease of L_c by about 10% for the lowest annealing temperature (T_a = 250 °C) when going from the shortest to the longest macromolecules. L_1 increases by as much as 100% at constant annealing temperature over the investigated molecular weight range (Figure 11). This is obviously inconsistent with its assignment to the crystal thickness. The small variation of L_2 with the molecular weight at different T_a, if any, is compatible with $L_c = L_2$. (iii) It has been pointed out that the value of v_c^{lin} could not be lower than that of the weight degree of crystallinity W_c. It should, however, be noted that these quantities, although related, are not strictly equivalent. Moreover large errors can occur in their determination. Previous comparisons of v_c^{lin} and W_c were essentially made on a restricted range of degrees of crystallinity. Our data cover a wide range of degrees of crystallinity (0.2−0.6). Moreover, the preparation of the sample includes a nucleation step with many centers resulting in samples homogeneously filled with lamellar stacks. The comparisons between W_c^{WAXD} and $v_1^{lin} = L_1/(L_1 + L_2)$ and $v_2^{lin} = L_2/(L_1 + L_2)$ are displayed in parts a and b of Figure 12. Similar results are obtained using the values of W_c^{DSC}. If one assumed that $L_1 = L_c$ and hence took the corresponding values of v_1^{lin} as representing the linear degree of crystallinity, one would reach the conclusion that the latter increases with increasing molecular weight which would obviously contradict the WAXD and DSC results. One can reasonably expect that the linear degree of crystallinity v_c^{lin} and the macroscopic crystallinity will follow the same trend, which is consistent with our assignment of L_c to the smallest length L_2 obtained from the correlation function.

The major morphological change induced by an increase of the molecular weight is an increase of the thickness of the amorphous regions while the crystalline thickness seems to be only governed by the annealing temperature T_a. It was shown for other semicrystalline

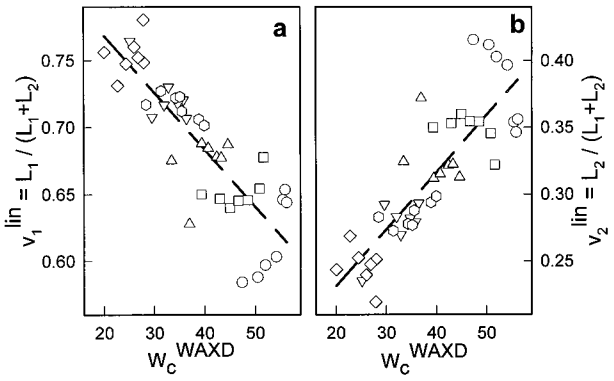

Figure 12. Comparison between W_c^{WAXD} and v_1^{lin} (a) and W_c^{WAXD} and v_2^{lin} (b) for the different PEEK samples (○) 4k, (□) 8k, (△) 18k, (▽) 32k, (◇) 79k, and (⬡) Stabar. The dashed line is the linear regression drawn through all the data as a guide for the eye.

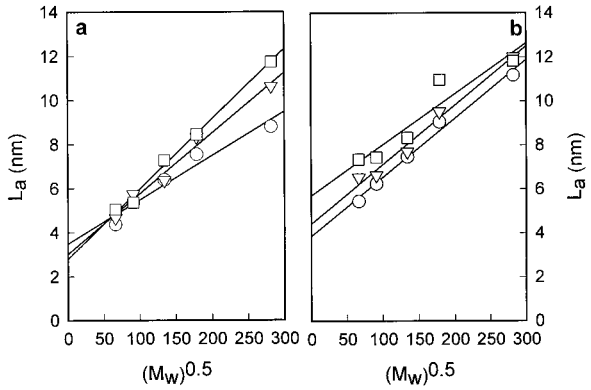

Figure 13. Thickness of the amorphous regions L_a against sample $(M_w)^{1/2}$ for the PEEK fractions annealed during 1 h from the glassy state at 250 (○), 280 (□), and 300 °C (▽) (a) and at 310 (○), 320 (□), and 330 °C (▽) (b).

polymers (polyethylene, polypropylene, poly(ethylene terephthalate) that the thickness of the amorphous regions, depends linearly on the average dimension of the polymer chain $r_w = \sum w_i M_i^{1/2}$ assimilated to an unperturbed random coil just before its crystallization.[43] For low polydispersity polymer samples, this average dimension r_w is proportional to the square root of weight average molecular weight. The thickness of the amorphous regions (L_a) is linearly proportional to $M_w^{1/2}$ as shown in Figure 13 for annealing temperatures between 250 and 330 °C. The linear correlation function analysis used throughout this work is based on the assumption that the lamellar stacks have a infinite lateral size. Electron microscopy data of PEEK and WAXD peak width analysis reveal that this is far from being the case. Therefore, it can be reasonably questionned whether the correlation function is suitable to accurately investigate the crystal morphology of very irregular PEEK lamellar systems.

Conclusions

The double melting behavior of semicrystalline narrow molecular weight PEEK fractions was found to be strongly dependent on the molecular weight. Mainly, the reorganization process occurring during the DSC scan was found to be hindered by the presence of entanglements in the amorphous zones. As a consequence the position of the high melting peak shifts to lower temperature with increasing molecular weight. In contrast, for given annealing conditions, the position

of the lower temperature endotherm is almost independent of the molecular weight, suggesting the existence of a very similar distribution of crystalline thicknesses in the various samples prior to the DSC scan. The correlation function analysis has been used to derive the amorphous and crystalline layer thicknesses and the linear degree of crystallinity from the SAXS data. On the basis of various findings, the crystalline thickness was attributed to the smallest of the two lengths obtained by this procedure. In particular, it was found that for constant annealing conditions the crystal thickness remains unaffected by a change of the molecular weight while the amorphous layer is found to strongly increase with increasing chain length due to the presence of entanglements. This leads to a decrease in the linear degree of cristallinity within the lamellar stacks which is quite consistent with the behavior of the macroscopic crystallinity. It seems that many morphological parameters such as the amorphous zone thickness and the degree of crystallinity are governed by the chain length and more precisely by the ability of a macromolecule to disentangle during its crystallization.

Acknowledgment. This work was supported by the Belgian National Funds for Scientific Research and the European Union through the HCMP Access to Large Installations Project, Contract CHGE-CT93-0040 to the E.M.B.L. The authors thank Dr. J. Rault for fruitful discussions.

References and Notes

(1) Attwood, T. E.; Dawson, P. C.; Freeman, J. L.; Hoy, L. R.; Rose, J. B.; Staniland, P. A. *Polymer* **1981**, *22*, 1096.
(2) Stening, T. C.; Smith, C. P.; Kimber, P. J. *J. Mod. Plast.* **1981**, 86.
(3) Galli, E. *Plast. Des. Forum* **1985**, March−April, 92.
(4) Blundell, D. J.; Osborn, B. N. *Polymer* **1983**, *24*, 953.
(5) Kumar, S.; Anderson, D. P.; Adams, W. W. *Polymer* **1986**, *27*, 329.
(6) Cheng, S. Z. D.; Cao, M.-Y.; Wunderlich, B. *Macromolecules* **1986**, *19*, 1868.
(7) Blundell, D. J. *Polymer* **1987**, *28*, 2248.
(8) Cebe, P.; Chung, S.; Hong, S. D. *J. Appl. Polym. Sci.* **1987**, *33*, 487.
(9) Lee, Y.; Porter, R. S. *Macromolecules* **1987**, *20*, 1336.
(10) Cebe, P. *J. Mater. Sci.* **1988**, 23, 3721.
(11) Bassett, D. C.; Olley, R. J.; Al Raheil, I. A. M. *Polymer* **1988**, *29*, 1745.
(12) Lee, Y.; Porter, R. S.; Lin, J. S. *Macromolecules* **1989**, *22*, 1756.
(13) Mehmet-Alkan, A. A.; Hay, J. N. *Polymer* **1992**, *33*, 3527.
(14) Fratini, A. V.; Cross, E. M.; Whitaker, R. B.; Adams, W. W. *Polymer* **1986**, *27*, 861.
(15) Wakelyn, N. T., *Polym. Commun.* **1984**, *25*, 306.
(16) Rueda, D. R.; Ania, F.; Richardson, A.; Ward, I. M.; Balta-Calleja, F. J. *Polym. Commun.* **1983**, *24*, 258.
(17) Hay, J. N.; Kemmisch, D. J.; Langford, J. I.; Rae, A. I. M. *Polym. Commun.* **1984**, *25*, 175.
(18) Wakelyn, N. T. *J. Polym. Sci., Polym. Lett.* **1987**, *25*, 25.
(19) Hay, J. N.; Langford, J. I.; Lloyd, J. R. *Polymer* **1989**, *30*, 489.
(20) Zimmermann, H. J.; Konnecke, K. *Polymer* **1991**, *32*, 3162.
(21) Iannelli, P. *Macromolecules* **1993**, *26*, 239.
(22) Wang, J.; Alvarez, M.; Zhang, W.; Wu, Z.; Li, Y.; Chu, B. *Macromolecules* **1992**, *25*, 6943.
(23) Hsiao, B. S.; Gardner, K. H.; Wu, D. Q.; Chu, B. *Polymer* **1993**, *34*, 3986.
(24) Hsiao, B. S.; Gardner, K. H.; Wu, D. Q. *Polymer* **1993**, *34*, 3996.
(25) Krüger, K.-N.; Zachmann, H. G. *Macromolecules* **1993**, *26*, 5202.
(26) Jonas, A. M.; Russell, T. P.; Yoon, Do Y. *Macromolecules* **1996**, *28*, 8491.
(27) Fougnies, C.; Damman, P.; Villers, D.; Dosière, M.; Koch, M. *Macromolecules* **1997**, *30*, 1385.
(28) Fougnies, C.; Damman, P.; Dosière, M.; Koch, M. H. J. *Macromolecules* **1997**, *30*, 1392.
(29) Hinkley, J. A.; Eftekhari, A.; Crook, R. A.; Jenson, B. J.; Singh, J. J. *J. Polym. Sci., Part B* **1992**, *30*, 1195.
(30) Nishino, T.; Tada, K.; Nakamae, K. *Polymer* **1992**, *33*, 736.
(31) Jones, D. P.; Leach, D. C.; Moore, D. R. *Polymer* **1985**, *26*, 1385.
(32) Chivers, R. A.; Moore, D. R. *Polymer* **1994**, *35*, 110.
(33) Lovinger A. J., Davis D. D. *Polym. Commun.* **1985**, *26*, 322.
(34) Lovinger A. J., Davis D. D. *J. Appl. Phys.* **1985**, *58*, 2843.
(35) Lovinger A. J., Davis D. D. *Macromolecules* **1986**, *19*, 1861.
(36) Olley, R. H.; Bassett, D. C.; Blundell, D. J. *Polymer* **1986**, *26*, 344.
(37) Chung, C. T.; Chen, M. *Polym. Prepr.* **1992**, *33*, 420.
(38) Zhang, Z.; Zeng, H. *Makromol. Chem.* **1992**, *193*, 1745.
(39) Zhang, Z.; Zeng, H. *Polymer* **1993**, *34*, 1551.
(40) Zhang, Z.; Zeng, H. *Polymer* **1993**, *34*, 4032.
(41) Strobl, G. R.; Schneider, M. J. *J. Polym. Sci., Polym. Phys. Ed.* **1980**, *18*, 1343.
(42) Strobl, G. R.; Schneider, M. J.; Voigt-Martin, I. G. *J. Polym. Sci., Polym. Phys. Ed.* **1980**, *8*, 1361.
(43) Rault, J.; Robelin-Souffaché, E. *J. Polym. Sci., Polym. Phys. Ed.* **1989**, 27, 1349.
(44) Mandelkern, L.; Alamo, R. G.; Kennedy, M. A. *Macromolecules* **1990**, *23*, 4721.
(45) Cebe, P., *J. Mater. Sci.* **1988**, *23*, 3721.
(46) Jonas, A.; Legras, R.; Scerrenberg, R.; Reynaers, H. *Macromolecules* **1993**, *26*, 526.
(47) Waddon, A. J.; Keller, A.; Blundell, D. J. *Polymer* **1992**, *33*, 27.
(48) Day, M.; Deslandes, Y.; Roovers, J.; Suprunchuk, T. *Polymer* **1991**, *32*, 1258.
(49) Deslandes, Y.; Sabir, F.-N.; Roovers, J. *Polymer* **1991**, *32*, 1267.
(50) Roovers, J.; Cooney, J. D.; Toporowski, P. M. *Macromolecules* **1990**, *23*, 1611.
(51) Bas, C.; Battesti, P.; Albérola, N. D. *J. Appl. Polym. Sci.* **1994**, *53*, 1745.
(52) Sichina, W. J. *24th NATAS Conf., Proc.* **1995**, 375.
(53) Information and demonstration of the "X-ray" software are available on the WEB site of the Université de Mons-Hainaut: www.umh.ac.be/~POLY/INDEX.HTML.
(54) Koch M. H. J. and Bordas, J. *Nucl. Inst. Methods* **1983**, *A208*, 461.
(55) Boulin C. F.; Kempf R.; Gabriel A.; Koch M. H. J. *Nucl. Instr. Methods* **1988**, *A269*, 312.
(56) Balta-Calleja, F. J.; Vonk, C. G. In *X-ray Scattering of Synthetic Polymers*; Elsevier: Amsterdam, 1989; Chapter 7.
(57) Eisele, U. *Introduction to Polymer Physics*; Springer-Verlag: New York, 1990.
(58) Vaughan, A. S.; Stevens, G. C. *Polymer* **1995**, *36*, 1531.
(59) Xin Lu, S.; Cebe, P.; Capel, M. *Macromolecules* **1997**, *30*, 6243.
(60) Hoffmann, J. D.; Weeks, J. J. *J. Res. Natl. Bur. Stand. (U.S.)* **1962**, *66A*, 13.
(61) Alexander, L. E. *X-ray Diffraction Methods in Polymer Science*; John Wiley and Sons: New York, 1954.
(62) Zimmermann, H. J.; Könnecke, K. *Polymer* **1991**, *32*, 3162.
(63) Chen, F. C.; Choy, C. L.; Wong, S. P.; Young, K. *J. Polym. Sci., Polym. Phys. Ed.* **1981**, *19*, 971.

MA980640A